ACS NANO

www.acsnano.org

ARTICLE

Probing Protein Corona Formation around Gold Nanoparticles: Effects of Surface Coating

Narjes Dridi, Zhicheng Jin, Woody Perng, and Hedi Mattoussi*

Cite This: *ACS Nano* 2024, 18, 8649–8662

Read Online

ACCESS | Metrics & More | Article Recommendations | Supporting Information

ABSTRACT: **There has been much interest in integrating various inorganic nanoparticles (nanoscale colloids) in biology and medicine. However, buildup of a protein corona around the nanoparticles in biological media, driven by nonspecific interactions, remains a major hurdle for the translation of nanomedicine into clinical applications. In this study, we investigate the interactions between gold nanoparticles and serum proteins using a series of dihydrolipoic acid (DHLA)-based ligands. We employed gel electrophoresis combined with UV−vis absorption and dynamic light scattering to correlate protein adsorption with the nature and size of the ligand used. For instance, we found that AuNPs capped with DHLA alone promote nonspecific protein adsorption. In comparison, capping AuNPs with polyethylene glycol- or zwitterion-appended DHLA essentially prevents corona formation, regardless of ligand charge and size. Our results highlight the crucial role of surface chemistry and core material in protein corona formation and offer valuable information for the design of colloidal nanomaterials for biological applications.**

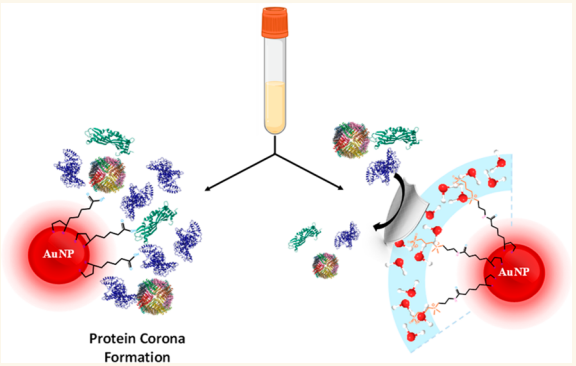

KEYWORDS: *Nanobio interface, protein corona, gold nanoparticles, surface engineering, adsorption kinetics*

1. INTRODUCTION

In recent years, inorganic nanocrystals have garnered significant attention for their potential applications in developing biotechnological kits, and as platforms for biodiagnosis and therapeutics.[1−7] Gold nanoparticles (AuNPs), in particular, have several tunable photophysical properties including size- and shape-dependent surface plasmon absorption properties, which can be exploited in optical sensor design, photothermal heating, and surface enhanced Raman scattering.[8,9] These properties make them highly attractive for use in biology and medicine.[10−12] However, integrating these nanocrystals into biological systems necessitates good long-term colloidal stability combined with compactness in overall size and controlled surface reactivity, in order to optimize such integration.[13−17] Unfortunately, most ubiquitously grown and tested AuNPs (e.g., citrate-coated) are poorly stabilized and tend to exhibit nonspecific interactions with proteins in biological media. This promotes the formation of a protein corona around the gold nanocolloids, which alters their functionality, affects their physiological fate, and enhances their toxicity when used in biological applications.[18−20]

At initial stages of developing nanomaterials for biomedical investigations, coating strategies had focused on addressing issues of colloidal stability of the nanocrystals in aqueous media while preserving their photophysical properties, in particular, under harsh physiological conditions. Subsequently, the challenges have shifted toward engineering a surface coating that also reduces or eliminates nonspecific interactions with biomolecules. For instance, Lequeux and co-workers employed single molecule diffusion dynamics to evaluate the role of the ligand in corona formation around luminescent quantum dots in the cytoplasm of living cells. Among others, they used single NP tracking to demonstrate that only QDs surface-coordinated with a sulfobetaine (SB)-based zwitterion polymer totally suppress protein corona formation.[21] In contrast, phosphocholine- and carboxybetaine-coated QDs undergo reversible protein adsorption or partial aggregation.

Protein corona is the term used to describe nonspecifically adsorbed proteins or other biomolecules onto poorly engineered nanoparticle surfaces, when introduced into a physiological environment.[22−29] This process introduces a complex and unpredictable "biological identity" to the nanocrystal that differs from the synthetic/chemical identity

Received: August 24, 2023
Revised: February 21, 2024
Accepted: February 28, 2024
Published: March 12, 2024

https://doi.org/10.1021/acsnano.3c08005
ACS Nano 2024, 18, 8649−8662

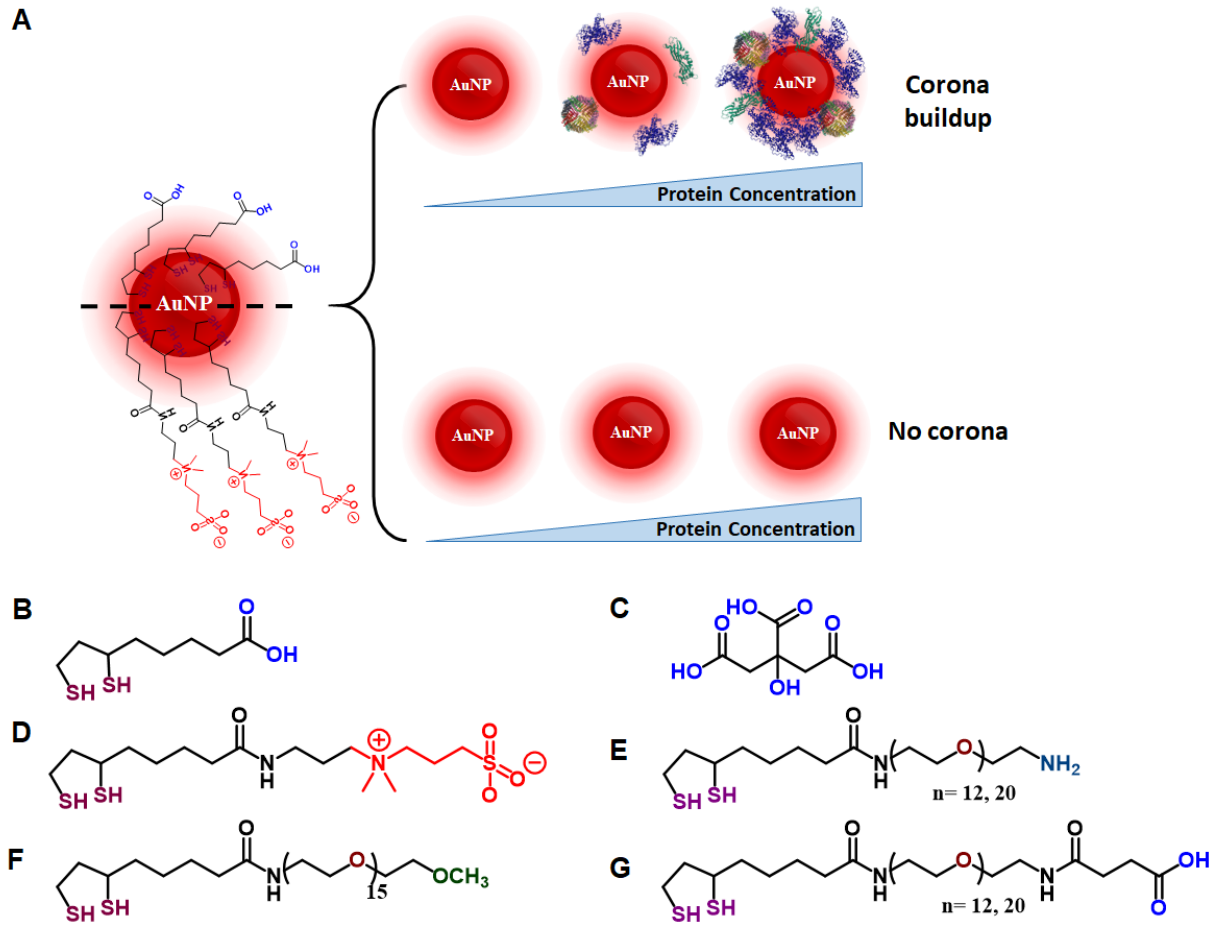

Figure 1. (A) Schematic representation of the effect of the surface chemistry on the interactions of the AuNPs with albumin, and the ensuing corona formation for DHLA-coating (top), or prevention of corona buildup (bottom) for zwitterion and PEGylated coatings. Chemical structures of the ligands used: (B) DHLA, (C) Citrate, (D) DHLA-ZW, (E) DHLA-PEG_{750}-OMe, (F) DHLA-PEG_{600}-NH_2, DHLA-PEG_{1000}-NH_2, (G) DHLA-PEG_{600}-COOH and DHLA-PEG_{1000}-COOH.

of the starting material.[30−33] It also alters the behavior of the nanocolloids, resulting in several side-effects such as lower targeting efficiency, reduced blood retention time, and enhanced disease-induced nanotoxicity.[34−39] Previous studies have shown that corona formation is influenced by a few key factors, including the nanoparticle size, shape, and composition, along with protein source, protein concentration, incubation time, and temperature.[40−44] Surface chemistry plays a crucial role in governing the interactions of nanocrystals with biomolecules.[26,45,46] Strategies like ligand exchange and encapsulation, along with using ligands with antifouling properties such as those presenting polyethylene glycol blocks, glycans, or zwitterion motifs have been shown to minimize corona buildup.[21,24,39,45,47−52] Given the recent growth of using nanomaterials integrated with biological systems, as nanoscale platforms to develop biosensors and diagnostic methods, a sound understanding of the interfacial properties of such platforms is still critically important. In particular, more investigation of the nonspecific adsorption of biomolecules (such as proteins in biological media) on nanocolloids stabilized with various ligand coating strategies and how to prevent that process are still needed.[53,54] This will allow us to gain additional in depth understanding of how the combined core material makeup, size, shape, and stabilizing ligands used can influence the corona buildup in complex media. It will also help researchers identify improved ligand designs that can best prevent corona formation, improve in vivo stability, and reduce toxicity of colloidal nanomaterials of interest.

In this study, we investigated the effect of surface chemistry on the formation of the protein corona around AuNPs surface-stabilized with dihydrolipoic acid (DHLA)-based ligands when exposed to bovine serum albumin (BSA), fetal bovine serum (FBS), or total serum protein as analogues for in vivo conditions. By analyzing the electrophoretic mobility of various surface-coated AuNPs, we found that nanocolloids stabilized with small ligands trigger protein adsorption and corona buildup, with associated effects of the overall size on the amount of adsorbed proteins. In addition, combining gel electrophoresis and dynamic light scattering, we found that introducing a PEG block or a zwitterion motif in the ligands can effectively prevent corona formation. These findings confirm the importance of surface chemistry in controlling protein corona formation and can guide the design of colloidal nanomaterials that are optimally adapted for use in biological applications.

2. RESULTS AND DISCUSSION

2.1. Rationale. Nonspecific adsorption of biomolecules such as proteins on colloidal nanocrystals can alter the net surface charge and endow the nanocolloids with enlarged

https://doi.org/10.1021/acsnano.3c08005
ACS Nano 2024, 18, 8649−8662

Table 1. Characteristics of 10 nm As-Grown OLA-AuNPs Side-by-Side with Those Subjected to Ligand Substitution with Various DHLA-Modified Ligands Used in This Study

ligand used	OLA (native)	DHLA-PEG$_{750}$-OMe	DHLA-PEG$_{600}$-NH$_2$	DHLA-PEG$_{600}$-COOH	DHLA-PEG$_{1000}$-NH$_2$	DHLA-PEG$_{1000}$-COOH	DHLA-ZW	DHLA-AuNPs
R_H(nm)	6.4	9.1	9.0	9.5	9.0	9.3	8.3	8.0
PDI[a]	0.04	0.08	0.06	0.02	0.1	0.1	0.1	0.2
SPR (nm)	521	521	522	521	521	521	521.5	518

[a]PDI is the polydispersity index extracted from fitting the autocorrelation function of the scattered signal (see Supporting Information). PDI ≤ 0.1 observed essentially for all samples implies a size distribution ($\Delta R_h/R_h$) ≤ 10%.

overall dimensions that account for the native core plus the newly adsorbed proteins. These two effects can be accounted for by tracking changes in the electrophoretic mobility of the nanocolloid migration in low density cross-linked polymers, such as an agarose gel. It was shown in early work by Rodbard and Chrambach in 1970 that the electrophoretic mobility, M, measured for any migrating species (e.g., a nanoparticle) through a gel under applied electric voltage depends on the gel concentration, Φ, following the expression.[55−57]

$$\log_{10}(M) = \log_{10}(M_0) - K_R\Phi \quad (1)$$

where M_0 refers to particle mobility in the absence of the gel, and the retardation coefficient (or slope of the line), K_R, is constant for any specified charged molecule and for constant cross-linking percentage of the gel. Furthermore, interactions with the gel network yields retardation coefficient that exhibits a strong dependence on the particle size. In particular, it was reported that K_R varies linearly with the particle size for low-concentration gels like those made of one-dimensional fiber polymers such as agarose gel.[55,56]

We take advantage of these properties and use gel mobility measurements to extract valuable information about the correlation between surface coating and corona formation on spherical gold nanoparticles of different sizes. The nanoparticles are stabilized with different coordinating molecules via ligand exchange reaction. More precisely, we use three sets of AuNPs. One set (10 nm dimeter) is grown under hydrophobic conditions with a native coating made of oleylamine, reported by Swihart and co-workers.[58] The average diameter for our NPs was extracted from TEM measurements.[59] The other two are citrate-stabilized 5 and 30 nm diameter NPs and have been grown in aqueous solutions, as reported by Puntes and co-workers.[60,61] Those authors have built on the original growth strategy developed by Turkevich and Frens using citrate ligands to control the NP diameter over a broad size range.[62,63] We should note that the above size range of NPs is comparable to the dimensions of most serum proteins (TEM images of the various AuNPs before and after ligand substitution are provided in the Supporting Information, Figure S1).[64,65]

In this study, we rely on the ligand exchange strategy using dihydrolipoic acid (DHLA)-based coordinating ligands to transfer oleylamine- or citrate-capped AuNPs to phosphate buffer saline (PBS) 1×, at pH 7.4, which mimics physiological conditions. The strong affinity of thiol-to-gold surfaces combined with the bidentate nature of the dithiolane groups, compared to their monothiol counterparts, reduces the rate of ligand desorption and results in a more stable coordination overall.[13,66] We tune the surface chemistry by modifying the size and structure of the hydrophilic motif, which affects the surface charge, hydrodynamic radius, the colloidal stability, and the interactions of the nanoparticles with native proteins in biological media. For instance, incorporating functional groups such as amine, carboxyl, and methoxy into the ligand structure endows the NPs with positive, negative, or neutral surface charge under physiological conditions; hence, the structures of ligands affect NP interactions with water and other surrounding molecules. Figure 1 provides a summary of the ligand structures used in this study. Characterization of the AuNP dispersions before and after ligand exchange using TEM imaging, ^{1}H NMR and FT-IR spectroscopy, along with UV−vis absorption and dynamic light scattering measurements is summarized in Table 1 and the Supporting Information, Table S1 and Figures S1−S6. The molar concentrations of the AuNPs used for our electrophoresis experiments were chosen to provide strong enough SPR signals that allow visualization of the mobility bands in the gel, while guaranteeing dilute conditions (large average separation distances between the NPs in the medium). Lower concentrations were used for larger size NPs, in order to maintain comparable overall solute surfaces for the various NP dispersions.

Our approach to evaluating corona formation relies on measuring changes in the mobility shift of the nanocolloids in agarose gel, when mixed with different molar equivalence of bovine serum albumin (BSA). Since the shift in the electrophoretic gel mobility is strongly affected by the net surface charge and overall size of the NPs, such a property can be easily altered by corona formation, where adsorption of proteins would increase their size and alter their surface charge. These properties make gel electrophoresis an informative tool for understanding corona formation around nanocolloids. Overall, we varied the concentration of BSA added to the dispersion from 0 to 200 μM. This allowed us to investigate nonspecific protein-to-NP interactions at concentrations relevant to those used in both *in vitro* and *in vivo* experiments. The mobility bands have been imaged by exploiting the typical reddish-pink color emanating for the surface plasmon resonance signature of spherical AuNPs, under white light exposure.

2.2. Protein Corona Buildup Around DHLA-Stabilized AuNPs. *2.2.1. Developing Saturation Profiles for Corona Proteins.* We start with 10 nm diameter AuNPs, grown under hydrophobic conditions using a high temperature reaction, where the native oleylamine coating is substituted with dihydrolipoic acid. The latter is a small molecule made of a short hydrophobic alkyl chain appended with two thiol groups at one end and a carboxylic acid group at the other end; DHLA promotes water solubility of the nanocrystals but only under basic conditions (pH ≥ 7).[67] Additionally, its ability to endow long-term stability to large size nanocolloids is rather limited.[17,68] Here, DHLA coating provides a good reference system for acquiring valuable data on corona formation around a set of AuNPs coated with other DHLA-based ligands, which have been applied in biology.[69−74] Figure 2A shows

https://doi.org/10.1021/acsnano.3c08005
ACS Nano 2024, 18, 8649−8662

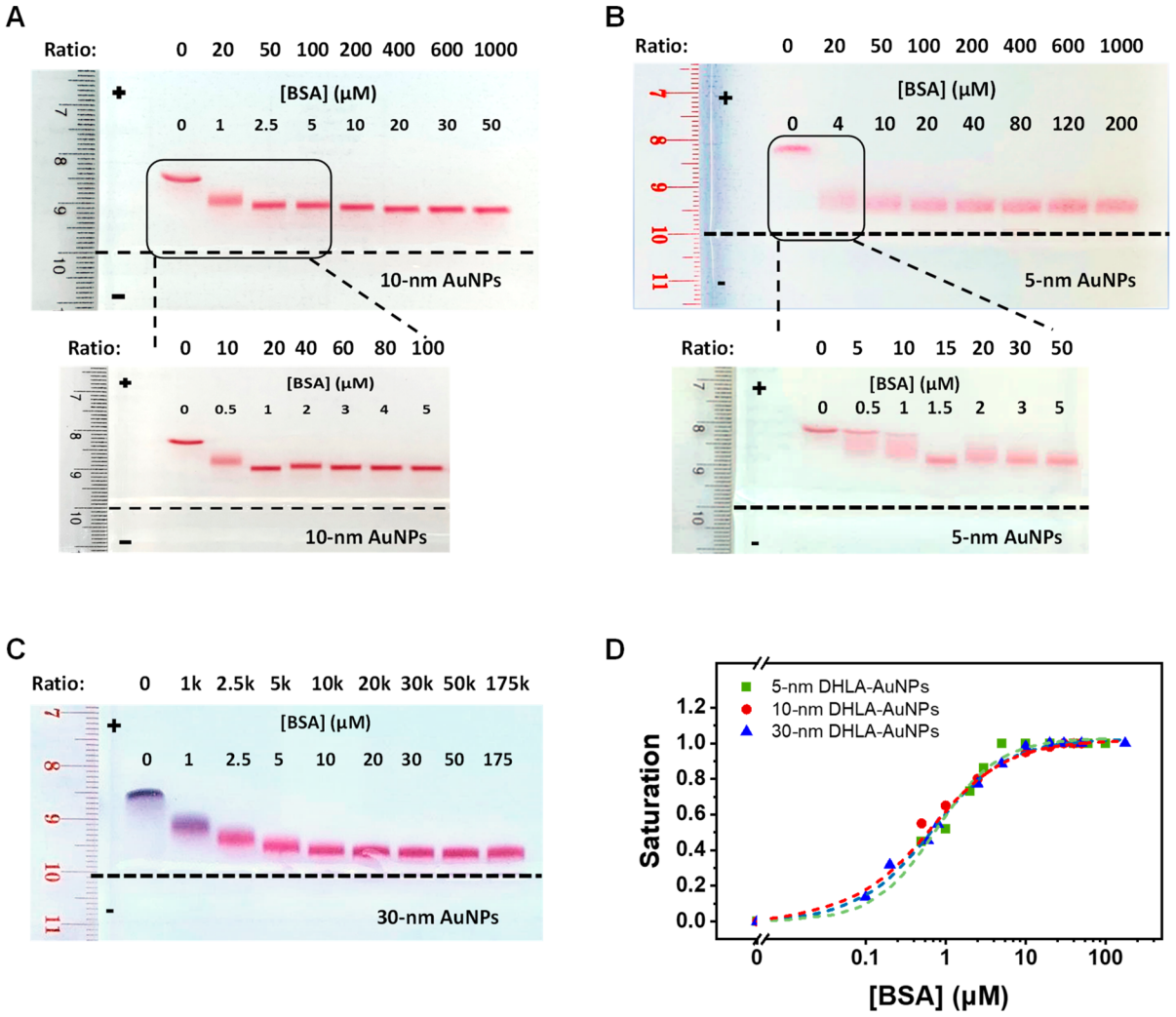

Figure 2. Agarose gel electrophoresis images collected from various size DHLA-stabilized AuNPs, showing progression of the mobility shift with the [BSA]/[AuNP] molar ratio used. The positive and negative signs (on the left) represent the anode and cathode, whereas the dashed line shows the loading wells. The data shown are for (A) 10 nm, (B) 5 nm, and (C) 30 nm diameter NPs. Insets showing expanded gel images spanning smaller [BSA] ranges are placed below the main gels in panels A and B. The dispersions were incubated with BSA for 30 min at room temperature. (D) Plot of the saturation, *S*, as defined in eq 2, vs [BSA], extracted from the gel data shown in panels A, B, and C. The dashed lines are fits to eq 3. We note that the band in wells 1 and 2 in the gel in panel C appears slightly blueish, which is due to interactions with the TBE buffer used in the gel electrophoresis experiment. This can result in slight destabilization of the dispersions. However, the band regains its pinkish color after mixing with BSA, suggesting a beneficial effect of protein adsorption on the NPs.

representative gel images acquired from dispersions of AuNPs which have been incubated with BSA in PBS buffer at a molar excess ranging from 0:1 to 1000:1 for 30 min at room temperature. The image shows that the pure DHLA-AuNP dispersion experiences the largest mobility shift toward the anode (lane 1 in the gel), a result attributed to the net negative surface charge of the AuNPs endowed by the terminal COOH groups in the coating. Additionally, a narrow mobility band is formed, implying that a single population of nanocolloids characterizes the DHLA-AuNP dispersion. As the concentration of BSA increases, the mobility shift progressively decreases and eventually saturates at ∼20 μM, corresponding to a [BSA]/[AuNP] molar ratio of 400:1. This is indicative of a change in the size and/or charge of the AuNPs that directly depends on BSA concentration. The gel data also show that the most pronounced changes occur within the range of molar ratios between 0:1 and 20:1. We also note smearing of the migration band for the smaller excess ratio (i.e., 10:1), which is indicative of a heterogeneous distribution of albumins around the AuNPs.[75] Here, variation in the number of bound proteins per NP manifests in different but close-spaced electrophoretic mobility shifts for the same sample, producing a broadened and smeared overall band. Variation in the number of self-assembled adsorbed (or coordinated) proteins around a NP can be described using a Poisson distribution function, the effects of which are drastic at low valence (low protein-to-NP ratio), as detailed in reference 75.

Next, we investigate the effects of varying the nanoparticle size by expanding the gel electrophoresis experiments to 5 and 30 nm diameter DHLA-AuNPs, prepared via ligand exchange starting with citrate-NPs introduced above. We note that the size range of our three sets of AuNPs is overall comparable to those measured for most serum proteins.[64,65] Small size AuNPs have lately drawn growing interest for use in *in vivo* applications.[2,76−78] Figure 2B,C show that changes (i.e., reduction) in the mobility shift are most pronounced for

https://doi.org/10.1021/acsnano.3c08005
ACS Nano 2024, 18, 8649−8662

lower [BSA] before reaching saturation at higher protein concentrations, a trend comparable to the one observed for the 10 nm NPs. Nonetheless, the migration bands for both sets are slightly broader than those measured for the 10 nm NPs. A more pronounced smearing at low molar ratios can also be seen in those gels, which is indicative of the presence of heterogeneous population of NPs with a varying number of adsorbed proteins, as discussed above. Additional subtle differences in the progression of the mobility data toward saturation measured for the different sets of AuNPs exist. Namely, saturation requires higher molar excess of proteins for larger NP diameters (i.e., NPs with larger surfaces), see Figure 2A–C.

We attribute the measured changes in mobility shift of AuNPs migrating through the gel network to surface-adsorbed proteins. One can thus exploit the dependence of the mobility changes as a function of [BSA] to extract a saturation curve that accounts for the BSA binding affinity to each set in the three DHLA-AuNPs tested. Such a curve can be generated from the mobility data shown in Figure 2 using the relationship:[24]

$$S = \frac{d_0 - d}{d_0 - d_{sat}} \tag{2}$$

where d_0, d, and d_{sat} respectively represent the migration distance of the AuNP band from the loading well in the absence of proteins (i.e., [BSA] = 0 μM), at a given value of [BSA] and at saturation concentration. An S-shaped plot is generated for all three sets of NPs, which can be fit using the Hill function expressed as[79]

$$y = a \times \frac{[\mathrm{BSA}]^n}{K_d + [\mathrm{BSA}]^n} \tag{3}$$

Such a fit provides values for the apparent dissociation constant (K_d) and the Hill coefficient (n), see the dashed line in Figure 2E. These values yield information about the protein concentration corresponding to 50% saturation and the cooperativity mode of protein binding onto the NPs, respectively.[80,81] The values for the Hill coefficient, n, and the dissociation constant, K_d, deduced from fits to the saturation data for all three sets of AuNPs are summarized in Table 2. The values extracted for the Hill coefficient imply that protein adsorption onto DHLA-capped AuNPs is essentially noncooperative for all three sets of NPs.[80] The value for K_d extracted from fitting the mobility data is essentially comparable for all three sets of AuNPs. They are also close to the values we reported for corona buildup around luminescent, DHLA-stabilized CdSe-ZnS QDs for which $K_d \sim 0.96$ μM was measured.[24]

Table 2. Thermodynamics Parameters for the Nonspecific Adsorption of BSA onto DHLA-AuNPs of Different Size[a]

DHLA-AuNPs	[AuNPs] (nM)	n	K_d (μM)	ΔG (kJ/mol)	number of BSA per NP at saturation
5 nm diameter	100	1.1	0.74	−35	15
10 nm diameter	50	0.91	0.65	−35	27
30 nm diameter	1	0.95	0.70	−35	

[a]The concentrations for the AuNPs used in the gel measurements were 100 nM (for 5 nm), 50 nM (for 10 nm), and 1 nM (for 30 nm).

The above mobility data are corroborated by dynamic light scattering measurements, which were limited to 10 nm DHLA-AuNPs incubated with varying concentrations of BSA for 30 min. Corona formation was evaluated by tracking changes in the hydrodynamic radius, R_H, as a function of [BSA]. We note that lower concentration of NPs and BSA (compared to those used in the gel electrophoresis experiments) were employed, as strong enough scattering intensities can be generated and effectively exploited for DLS measurements and analysis.[57,82] Additional details about DLS are provided in the Supporting Information, see Figure S6. Figure 3A,B show representative histograms of the intensity vs R_H extracted from the scattered intensity profiles for several molar excesses of BSA. Data show that even though a single peak profile has been measured for all conditions tested, indicating an absence of aggregate formation, there is pronounced broadening of the histograms which manifests in a larger polydispersity index (PDI) for

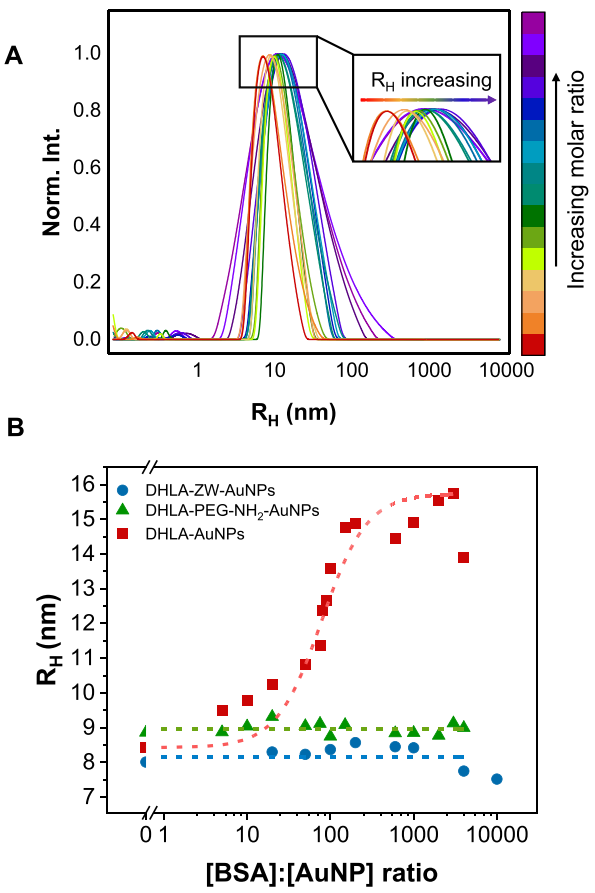

Figure 3. Changes in the hydrodynamic radius, R_H, measured for AuNPs with different ligand coatings following incubation for 30 min with varying BSA-to-AuNP molar ratios. (A) Histogram of the hydrodynamic radius of DHLA-AuNPs (10 nm) incubated with increasing BSA-to-AuNP molar ratios. The color scale at the right shows increasing [BSA]/[AuNP] from 0:1 to 4000:1. Inset shows the peak shift as well as broadening indicative of progressive protein adsorption around the AuNPs. (B) Plot of R_H of DHLA-, DHLA-ZW-, and DHLA-PEG$_{600}$-NH$_2$-capped AuNPs vs [BSA]/[AuNP] ratios. Dashed lines are guidelines drawn through data.

https://doi.org/10.1021/acsnano.3c08005
ACS Nano 2024, 18, 8649–8662

samples with a higher [BSA] compared to the starting AuNP dispersion (see Figure 3A). These features imply that larger R_H values are measured for the AuNPs incubated with increasing [BSA]. Notably, an S-shaped curve for R_H vs [BSA] has been extracted from the DLS data (Figure 3B). The larger value for the hydrodynamic radius measured at saturation, $R_H \sim 15.7$ nm, compared to the one measured for the AuNP only sample ($R_H \sim 8.4$ nm), accounts for the contribution of the surface adsorbed BSA; i.e., there is a protein corona buildup with a thickness of ~7.3 nm (see Table 3). We note that the above thickness should not be simply viewed as the static diameter of the proteins, because the hydrodynamic radius accounts for the effects of hydrodynamic interactions between diffusing solute objects (here AuNP-plus-corona).[83]

Table 3. Hydrodynamic Radius Extracted from DLS Data Shown in Figure 3, Using 10 nm Diameter AuNPs That Have Been Ligand Exchanged from OLA to Various DHLA-Modified Ligands

measured R_H (nm)	[AuNP] (nM)	R_H (nm) in absence of BSA	R_H (nm) in the presence of BSA at saturation	estimated corona thickness (nm)
DHLA-AuNPs	10	8.4	15.7	7.3
DHLA-PEG_{750}-OMe-AuNPs	10	9.0	9.1	none
DHLA-PEG_{600}-NH_2-AuNPs	10	8.9	9.0	none
DHLA-ZW-AuNPs	10	8.0	8.9	none

The above data on the equilibrium constant can be used to extract an estimate for the change in the free energy, ΔG, associated with the adsorption reaction of BSAs onto the DHLA-AuNPs, using the thermodynamic relation:[84]

$$\Delta G = RT \ln K_d \quad (4)$$

where R is the ideal gas constant and T is the temperature. This provides the means to correlate changes in the free energy of the system to the NPs used.[84,85] The ΔG values deduced for three sets of NPs (shown Table 2) are negative for all three sets of AuNPs. They indicate that for all three NPs the formation of an NP−protein complex is energetically favorable and thus spontaneous.

2.2.2. Modeling the Protein Packing around DHLA-Stabilized AuNPs. From the thermodynamic definition of the dissociation constant, one can deduce an estimate for the concentration at saturation for all three sets of AuNPs:[81]

$$K_d \sim [\text{BSA}] \text{ at } 50\% \text{ saturation} \Rightarrow [\text{BSA}]_{sat} \sim 2 \times K_d \quad (5)$$

Using the experimental data shown in Figure 2 and normalizing with the respect to the [AuNP] in the samples, we can deduce a value for the number of BSAs adsorbed around an individual AuNP for each set under the used conditions. We deduce that at saturation there are 15 and 27 BSAs in the corona layer around one individual nanocrystal for the 5 nm and 10 nm (see Table 2).

We now attempt to model the number of BSAs in a corona layer around an individual AuNP using close-packed protein arrangement. Under these conditions, the total number of BSAs surrounding a AuNP in a monolayer is given by the expression:[67,86]

$$N_{BSA} = 0.65 \times \left(\frac{(R_{tot}^3 - R_{NP}^3)}{R_{BSA}^3} \right) \quad (6)$$

where R_{NP} is the radius of DHLA-AuNPs, R_{BSA} is the average radius of BSA, and $R_{tot} = R_{NP} + 2 \times R_{BSA}$. To account for the steric considerations, a filling factor $\varphi = 0.65$ is used, corresponding to approximating BSA as a hard prolate spheroid.[67,87] Here, a sphericity value of 0.996 was used, see Supporting Information.

When using a close-packed model for the adsorbed proteins around the NPs, we consider the anisotropic structure of protein. A BSA molecule has an elongated conformation (i.e., an ellipse or an elongated ellipsoid) with a large dimension, L = 14 nm, and smaller dimension, l = 4 nm.[88] Given this asymmetry, the overall thickness of the corona layer and the number of proteins within will depend on how those proteins ultimately adsorb on the NP surfaces. In the simplest description, three distinct configurations can be envisioned, namely, those where BSAs absorb on the nanocrystal surface via their transversal plane, their longitudinal plane, or a stoichiometric mixture of the two (see Figure 4A−C). The schematics shown in Figure 4 indicate that the packing model with BSA adsorbing on the NP via the lowest dimension (i.e., standing proteins) yields the highest number of bound proteins, while the one having proteins laying flat on the NP surface yields the lowest number. However, a stoichiometric mixture of transversal and longitudinal packing is more realistic for the present system. Under these conditions, the model suggests that there would be 15 and 31 BSAs packed around each nanocolloid for 5 and 10 nm AuNPs, respectively. These estimates are comparable to the experimental values (see Table 2). We did not apply the above analysis to the mobility data collected for the 30 nm DHLA-AuNPs, because the colloidal stability of these dispersions is rather limited, a property attributed to the fatty and thin coating provided by these molecules. The colloidal stability is primarily imparted by electrostatic interactions promoted by the terminal COOH groups. Additionally, a much lower NP concentration was used, which further weaken the dispersion colloidal stability given the dynamic nature of the ligand coordination on the NP surfaces. Rather a diffuse corona layer may be more descriptive of the protein adsorption on this set of nanocrystals.[41,89]

Our results are overall consistent with data reported in previous studies using only citrate-AuNPs, where the groups of Puntes and Nandi have separately reported that nonspecific protein adsorption onto smaller size NPs exhibit faster binding kinetics compared to adsorption onto larger ones.[41,89,90] Nandi and co-workers combined DLS measurements with molecular docking simulation to demonstrate that an increase in the size of citrate-AuNPs induces variation in albumin binding orientation, along with changes in its secondary structures. Additionally, circular dichroism spectroscopy measurements by the same group revealed that the secondary structure of proteins experiences pronounced changes following adsorption onto 10−15 nm size AuNPs. Our surface coating strategy, relying on ligand substitution with dithiol coordinating molecules, combined with the use of gel electrophoresis experiments complement the works reported by Puntes and Nandi's groups. For example, we found that using a dithiol coordinating DHLA ligand, which has higher affinity for gold

https://doi.org/10.1021/acsnano.3c08005
ACS Nano 2024, 18, 8649−8662

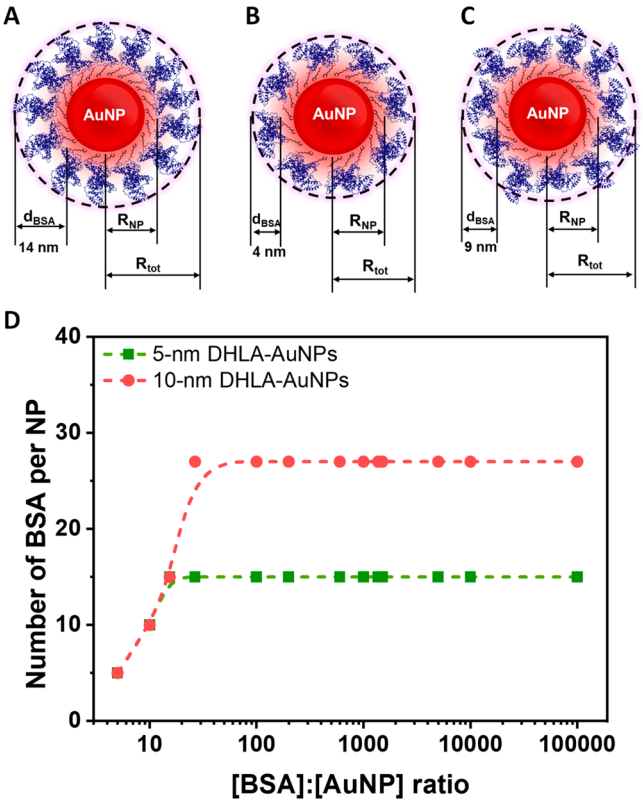

Figure 4. Schematic models for the corona layer thickness using the close-packed protein arrangement around the NP. Three configurations are shown: (A) Proteins are transversally arranged on the NP (adsorption occurring through the smaller cross-section), resulting in $d_{BSA} \cong 14$ nm. (B) Proteins are adsorbed via longitudinal cross-section, yielding $d_{BSA} \cong 4$ nm. (C) Proteins are adsorbed via a mixture of longitudinal and transversal cross sections, resulting in $d_{BSA} \cong 9$ nm. (D) Graphs showing the average numbers of BSAs in a corona layer around each NP as a function of the [BSA]/[AuNP] for the 5 and 10 nm AuNPs extracted from the gel data shown in Figure 2.

surfaces than citrate or CTAB molecules, but lacks a distinct hydrophilic motif, promotes corona formation on the AuNPs. However, insertion of a PEG block or a zwitterion motif in the coating completely alters the behavior of the system.

2.3. Preventing Corona Formation Using DHLA-PEG- and DHLA-Zwitterion Coatings. Several prior studies probing corona buildup around various nanocolloids using techniques such as DLS and ITC have suggested that protein affinity to nanomaterials depends on a variety of parameters, including surface charge and polarity of the coating ligands.[53,91−94] For instance, the binding affinity of BSA onto Au surfaces coated with self-assembled monolayers of alkylthiol molecules was found to depend on the terminal functional group, with the trend C_6H_5OH > CH_3 > COO^- > NH_4^+ > HO^- > oligoethylene glycol.[95] A few groups have reported that incorporating a polyethylene glycol (PEG) block into the ligand structure can reduce corona buildup on colloidal NPs.[45,96,97] Here, we test the ability of several coordinating ligands (which we have designed and synthesized) that combine a DHLA anchoring group and a hydrophilic motif to prevent corona buildup onto colloidal AuNPs. The ligands shown in Figure 1 present hydrophilic motifs that include a methyl ether terminated polyethylene glycol block with Mw = 750 Da (DHLA-PEG_{750}-OCH_3), a zwitterion (N,N-dimethylpropanediamine-sulfobetaine) group (DHLA-ZW), a COOH-appended DHLA-PEG_{600} (DHLA-PEG_{600}-COOH), a COOH-appended DHLA-PEG_{1000} (DHLA-PEG_{1000}-COOH), an amine-appended DHLA-PEG_{600} (DHLA-PEG_{600}-NH_2), and an amine-appended DHLA-PEG_{1000} (DHLA-PEG_{1000}-NH_2). They were used either pure or in combination(s) to prepare six sets of hydrophilic AuNP dispersions via ligand exchange of OLA-AuNPs with (1) pure DHLA-ZW (DHLA-ZW-AuNPs), (2) pure DHLA-PEG_{750}-OCH_3 (DHLA-PEG_{750}-OCH_3-AuNPs), (3) a ligand mixture of 70% DHLA-PEG_{750}-OCH_3 and 30% DHLA-PEG_{600}-COOH (DHLA-PEG_{600}-COOH-AuNPs), (4) a ligand mixture of 70% DHLA-PEG_{750}-OCH_3 and 30% DHLA-PEG_{1000}-COOH (DHLA-PEG_{1000}-COOH-AuNPs), (5) a ligand mixture of 70% DHLA-PEG_{750}-OCH_3 and 30% DHLA-PEG_{600}-NH_2 (DHLA-PEG_{600}-NH_2-AuNPs), and (6) a ligand mixture of 70% DHLA-PEG_{750}-OCH_3 and 30% DHLA-PEG_{1000}-NH_2 (DHLA-PEG_{1000}-NH_2−AuNPs). Dispersions 1 and 2, which are respectively prepared using a neutral PEG-OCH_3 and a charge balanced sulfobetaine, which present a net charge of zero, should in principle exhibit no migration band in the gel(s). Nonetheless, experimentally AuNPs and other nanocolloids stabilized with DHLA-ZW tend to exhibit a net negative zeta potential, which results from the differential binding of counterions in the surrounding medium onto the positive and negative groups of the zwitterion, following the concepts formulated in the hard/soft acid/base theory.[98] For instance, a zeta potential of −27 mV was recently reported for DHLA-ZW-AuNPs.[14] The various ligand exchanged AuNPs 1−6 were dispersed in PBS buffer. Aliquots of these dispersions were incubated with BSA at concentration ranging from 0 to 50 μM for 30 min, mixed with loading buffer and transferred to the gel wells. The loaded gels were then run under an applied electric field of 6 V/cm for 40 min. More details can be found in the Supporting Information. The gel images acquired for the various samples show a clear correlation between ligand structures and mobility shifts, see Figure 5. The images in Figure 5B show that while a minimal mobility shift toward the anode is recorded for all the DHLA-PEG_{750}-OCH_3-AuNP dispersions (bottom gel), the dispersions of DHLA-ZW-AuNPs exhibited a more pronounced mobility shift toward the anode for all wells, consistent with the larger negative zeta potential of ZW-coated NPs (top gel). The images in Figure 5D show that the mobility bands have consistently migrated toward the anode with the same mobility shifts for all BSA concentrations for both sets of DHLA-PEG_{600}-COOH-AuNPs and DHLA-PEG_{1000}-COOH-AuNPs, albeit a smaller shift was recorded for the coating with the larger PEG block (compare top and bottom gels). The gels for the DHLA-$PEG_{600/1000}$-NH_2-AuNP dispersions show migration toward the cathode for all BSA concentrations used (see Figure 5F).

Cumulatively, the above gel images show narrow and homogeneous migration bands, indicating that the AuNPs stayed monodisperse and essentially aggregate-free. More importantly, the gel data in Figure 5 acquired for all sets of AuNP coatings show one common trend: There is no change in the mobility shift with increasing [BSA], which can be attributed to absence of any nonspecific protein adsorption on AuNPs presenting any of the ligand combinations listed. The data also show mobility shifts that still reflect subtle effects of the nature of the hydrophilic motif and the terminal group, e.g., PEG size and COOH vs NH_2. The use of hydrophilic

https://doi.org/10.1021/acsnano.3c08005
ACS Nano 2024, 18, 8649−8662

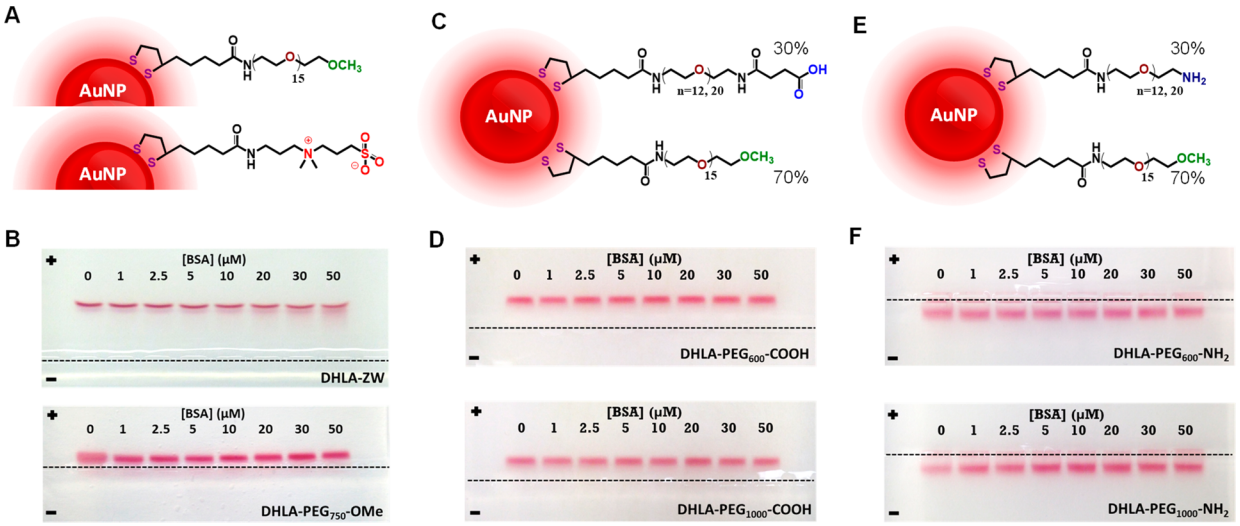

Figure 5. Effects of ligand size, structure, and surface charge on corona formation upon incubation with increasing BSA molar concentration, [BSA]. (A) Schematic representation of a DHLA-PEG$_{750}$-OMe-AuNP (top) and a DHLA-ZW-AuNP (bottom). (B) Gel images acquired from DHLA-ZW-AuNPs (top) and DHLA-PEG$_{750}$-OMe-AuNPs (bottom). (C) Schematic representation of a AuNP stabilized with a mixture of 30% DHLA-PEG$_{600/1000}$-COOH and 70% DHLA-PEG$_{750}$-OMe. (D) Gel images acquired from 30% DHLA-PEG$_{600}$-COOH-AuNPs (top) and from 30% DHLA-PEG$_{1000}$-COOH-AuNPs (bottom). (E) Schematic representation of a AuNP stabilized with a mixture of 30% DHLA-PEG$_{600/1000}$-NH$_2$ and 70% DHLA-PEG$_{750}$-OMe. (F) Gel images acquired from 30% DHLA-PEG$_{600}$-NH$_2$-AuNPs (top) and from 30% DHLA-PEG$_{1000}$-NH$_2$-AuNPs (bottom). The AuNPs were incubated with the indicated increasing [BSA]. Proteins and AuNPs were incubated for 30 min at room temperature.

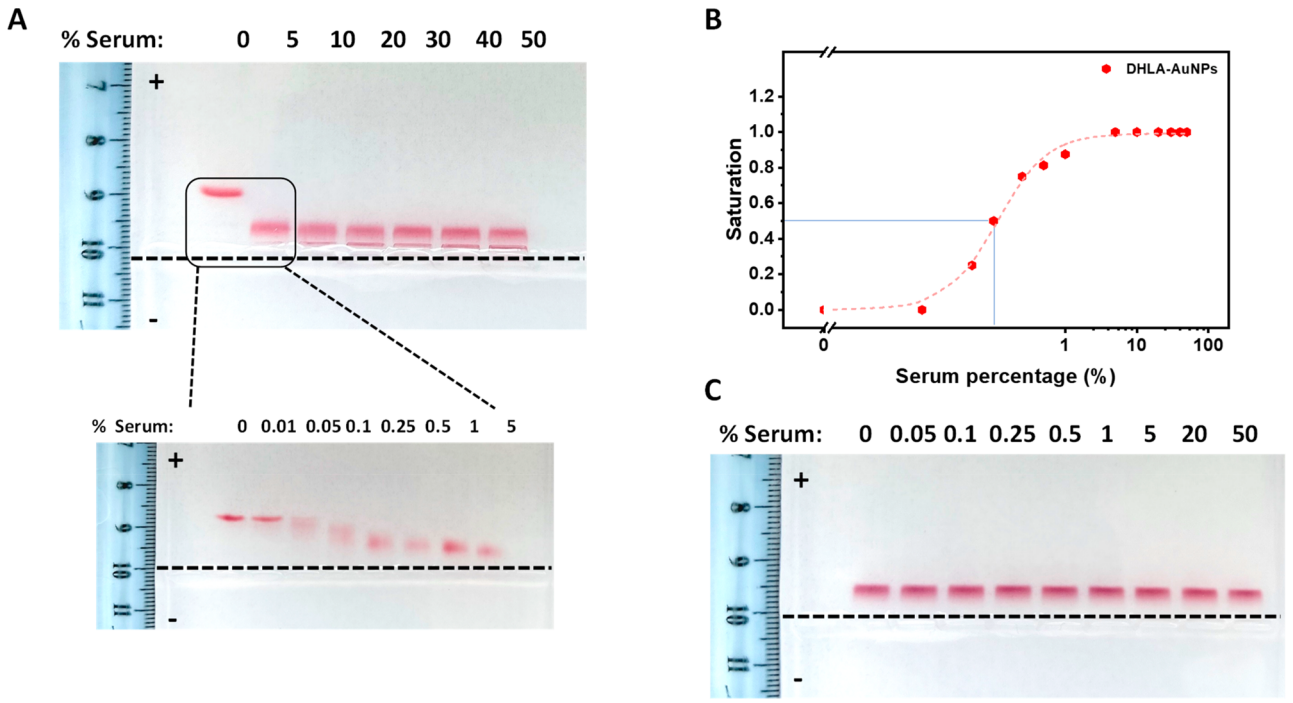

Figure 6. (A) Agarose gel images collected from DHLA-stabilized AuNPs showing progression of the mobility shift with % serum used. The inset shows an expansion of the 0−5% serum range. (B) Plot of the saturation, *S*, as defined in eq 2, vs % serum, extracted from the data in panel A. The dashed red line is a fit to eq 3; a value $n \sim 1.25$ was deduced from the fit. (C) Gel images collected from dispersions of DHLA-PEG$_{750}$-OCH$_3$-AuNPs vs % serum. The dispersions were incubated with serum for 30 min at room temperature. The positive and negative signs designate the anode and cathode, and the dashed black lines in panels A and C designate the loading wells.

PEG$_{600/1000}$ blocks has prevented corona buildup even when reactive COOH or NH$_2$ have been introduced. The net sign of mobility shift still accounts for the type of group inserted, COOH promotes migration toward the anode while amine promotes migration toward the cathode. Even though positively charged NH$_2$ groups tend to interact with cell membranes or proteins with an overall negative charge, our data show that insertion of a PEG$_{600/1000}$ block in the ligand has essentially eliminated any charge-facilitated nonspecific adsorption of proteins on AuNPs. This can be attributed to the highly polar nature of the PEG$_{600/750/1000}$ blocks which promote high affinity to water. We have indeed showed in

https://doi.org/10.1021/acsnano.3c08005
ACS Nano 2024, 18, 8649−8662

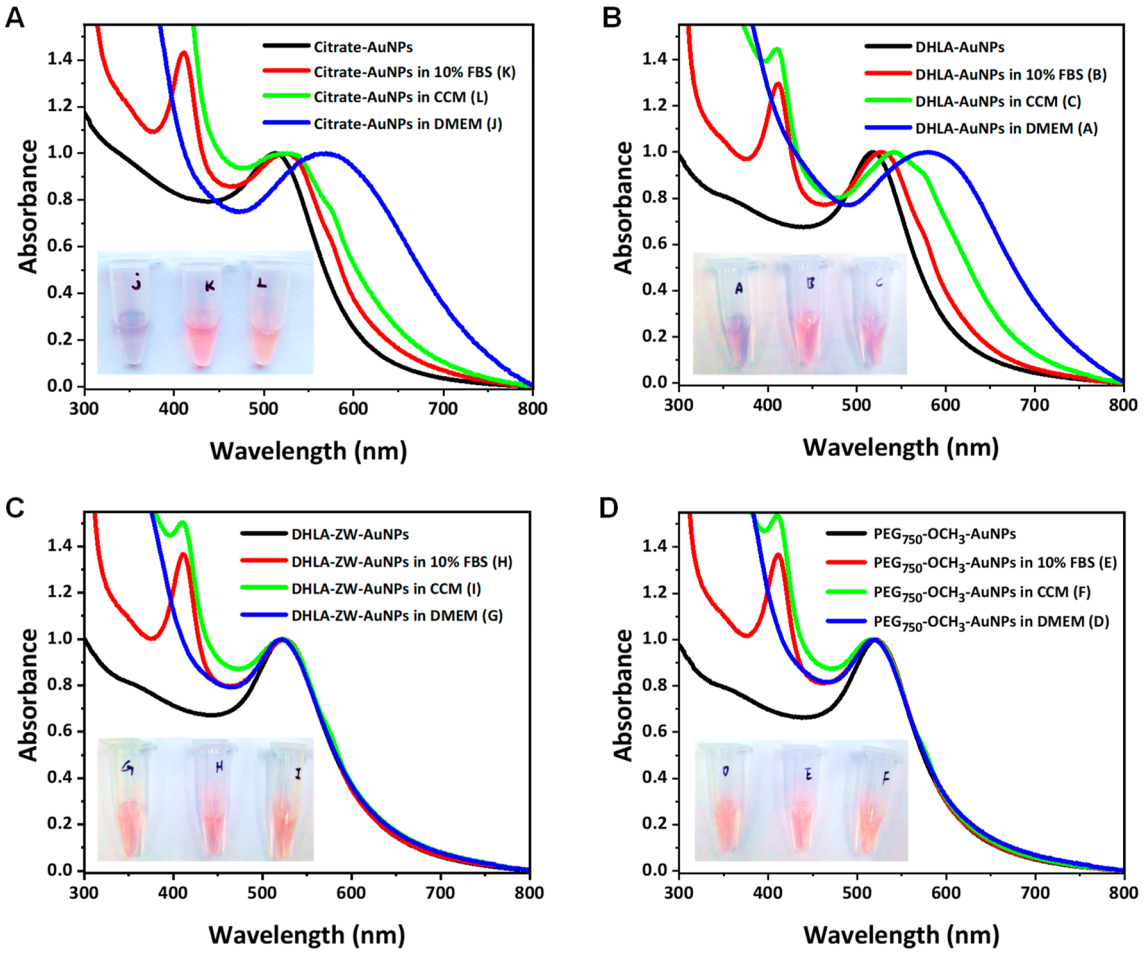

Figure 7. Absorbance spectra collected from 10-mm-path-length cells loaded with dispersions of (A) citrate-, (B) DHLA-, (C) DHLA-ZW-, and (D) DHLA-PEG$_{750}$OMe-stabilized AuNPs. The AuNPs were incubated with DMEM (tubes J, A, G, D), 10%FBS in PBS (tubes K, B, H, E), and CCM (tubes L, C, I, F). The black profiles are collected from AuNPs dispersed in water and serve as a control.

earlier work that PEG blocks with M_W = 400 Da or higher promote full dispersions of luminescent QDs in buffer media.[99] We note that luminescent CdSe-ZnS core−shell QDs stabilized with DHLA-PEG$_{600/1000}$-NH$_2$ showed low level corona formation as reported in a previous study.[24] This difference can be attributed to the stronger coordination interaction of DHLA-based ligands to AuNP surfaces, given the better matching of the soft-to-soft interactions between the Lewis base DHLA and Lewis acidic character of the AuNP surface. Coordination onto CdSe-ZnS core−shell QDs is weaker given the nature of the ZnS surface which exhibits a less soft Lewis acid. As such, a more stable coating of AuNPs promoted by DHLA-based ligands reduces nonspecific interaction with BSA. Finally, the ability of the rather compact ZW-appended ligands to prevent corona formation can be attributed to their strong interactions with water molecules and the generation of a stable hydration layer around the stabilized AuNPs. This renders it difficult to replace the layer of water molecules around the nanocrystals with proteins or other biomolecules; i.e., zwitterion motifs though compact are effective in substantially reducing nonspecific interactions with proteins.[100]

The above gels acquired for DHLA-ZW-AuNPs and DHLA-PEG-NH$_2$-AuNPs are further supported by DLS measurements as shown in Figure 3. The data show that the hydrodynamic radius of AuNPs stabilized with ZW and PEG-NH$_2$ coatings stayed constant when mixed with various concentrations of BSA, essentially confirming the prevention of any corona buildup around these AuNPs, compared to those prepared with DHLA coating.

We have expanded the above gel mobility experiments of AuNPs incubated with varying BSA concentrations in a PBS buffer to the configuration where incubation was carried out using a buffer containing an increasing % of serum. Serum is more representative of biological media as it contains several other biomolecules, in addition to the most abundant one, BSA. We carried out gel electrophoresis measurements using DHLA-AuNPs as well as DHLA-PEG-stabilized AuNPs. A representative gel summarizing the mobility shift experienced by DHLA-AuNPs shows an initial rapid reduction in the band migration measured for wells containing varying amounts of serum, followed by saturation at a higher % serum (see Figure 6). A saturation plot extracted from the gel data using eq 2 yields a sigmoidal curve similar to that shown in Figure 2D. Conversely, the gel image acquired from samples containing PEGylated-AuNPs instead shows no change in mobility shift with increasing % serum. These results confirm that DHLA coating promotes nonspecific adsorption of serum proteins that is commensurate with the % serum used. In comparison, no sign of corona formation was measured when using zwitterion-rich or PEGylated coating of the AuNPs.

https://doi.org/10.1021/acsnano.3c08005
ACS Nano 2024, 18, 8649−8662

2.4. Effects of the Coating on the Colloidal Stability of AuNPs in Biological Media. Successful integration within biological media requires that the nanoparticles be stable in physiological environments. Factors that impact such stability result from the balance of competitive effects of double-layer repulsive forces and van der Waals attractive forces, as stipulated by the Derjaguin−Landau−Verwey−Overbeek (DLVO) theory.[101]

In environments with high salt concentrations like PBS, Dulbecco's modified eagle's medium (DMEM), and cell culture medium (CCM), less colloidally stable nanoparticles would gradually develop small AuNP aggregates with time. However, if a protein corona rapidly forms around the nanoparticles, aggregation could be prevented as a result, due to the steric repulsions imparted by the adsorbed proteins, which now act as protecting/stabilizing coat. We hereby follow the protocols developed by Puntes and co-workers and use UV−vis optical absorption spectroscopy to characterize changes in the colloidal stability of AuNPs surface-capped with a few representative ligands, when dispersed in water, 10% fetal bovine serum (10% FBS in PBS), CCM (DMEM supplemented with 10% FBS), and DMEM.[41] More precisely, we used as-grown 10 nm citrate-stabilized dispersions, or started with OLA-grown AuNPs subsequently subjected to ligand substitution with DHLA, DHLA-PEG_{750}-OMe, and DHLA-ZW. It is known that the SPR peak location and shape can be affected by the dielectric constant of the surrounding medium as well as the interparticle distances, which has provided researchers with a tool for analyzing the interactions between nanocolloids and proteins in biological media and to use them for probing aggregation buildup.[12] Figure 7A,B show representative plots of the UV−vis absorption spectra collected from AuNPs capped with either citrate or DHLA ligands which have been incubated in three different media (10% FBS, CCM, and DMEM) for 30 min at room temperature, side-by-side with the pure AuNP dispersions; white light images of the dispersions in Eppendorf tubes are also provided. Spectra and images show that upon mixing with DMEM, both citrate- and DHLA-capped AuNPs aggregate into larger objects, resulting in a color change from red-pinkish to blue. There is a bathochromic shift combined with broadening of the SPR peak indicating the formation of a larger size of NP aggregates, as a result of the charge screening of the NP's surface ligands by the high salt concentration present in DMEM media. This gives a blueish color to the sample and results in a slight broadening and red shift of the SPR to ∼580 nm, as shown in Figure 7A and B. In comparison, when mixed with 10% FBS or CCM, the AuNP dispersions maintained their reddish-pink appearance. Additionally, the UV−vis absorption spectra showed a small red shift of the SPR peak position (with respect to the peak of the starting NP dispersion in water), compared to the one measured in DMEM. This can be attributed to the buildup of a protein corona layer around the AuNPs when incubated in 10% FBS or CCM, which alters the environment surrounding the NP surfaces, hence slightly shifting the plasmon resonance peak position and its width. Here, adsorption of proteins and other biomolecules available in the 10% FBS and CCM media reduces nanocrystal aggregation in high ionic salt media for the citrate/DHLA-AuNPs that are known to exhibit limited stability. The data acquired from DHLA-ZW- and DHLA-PEG_{750}-OMe-capped AuNPs (incubated with 10% FBS, CCM, and DMEM), in comparison, show that both the color of the AuNP dispersions and the SPR feature remained identical to those of the control sample, as shown in Figure 7C, D. We should note that the strong peak measured at ∼410 nm for the AuNPs mixed with 10% FBS or CCM is attributed to the absorption of the protein amino acids.

Overall, these results indicate that while a corona forms around citrate- and DHLA-capped AuNPs in 10% FBS and CCM, aggregation of the AuNPs was prevented by the adsorbed proteins. Here, the coronas provide strong enough steric repulsions that greatly improve the colloidal stability of the AuNPs. In this case, essentially the rate of corona formation is faster than the rate of NP aggregation. However, both DHLA-ZW- and DHLA-PEG_{750}-OMe-capped AuNPs exhibit excellent colloidal stability and improved protection against salt ions and serum biomolecules. The well-preserved SPR feature clearly confirmed the fact that the surface of the NPs was not altered by the proteins, indicating minimum-to-no protein adsorption.

3. CONCLUSIONS

We have investigated protein corona formation around spherical AuNPs with different surface-coatings using a few simple analytical techniques (e.g., agarose gel electrophoresis, UV−vis absorption spectroscopy, and dynamic light scattering). Our data show that AuNPs stabilized with small ligands (e.g., DHLA or citrate) promote nonspecific adsorption of proteins; these molecules tend to provide homogeneous solubility of the NPs in water via electrostatic repulsions. Gel electrophoresis combined with DLS measurements confirm corona formation, which tracks the molar concentration of the protein introduced, but the process can primarily be controlled by the nature and overall size of the ligands. In comparison, we find that appending hydrophilic motifs onto DHLA, such as PEG blocks or zwitterion groups, essentially eliminates nonspecific interactions, producing homogeneous dispersions that maintain colloidal stability as well as the characteristic reddish-pink color of plasmonic gold colloids for all conditions tested. Additionally, dispersions of as-grown citrate-NPs or ligand exchanged with DHLA interact strongly with media rich in salts like PBS or Dulbecco's modified eagle's medium (DMEM). This triggers gradual aggregation with time, as shown in the measured UV−vis absorption spectra (namely, the broad peak at 580 nm, blue profiles in panels A and B). However, rapid corona formation around citrate- or DHLA-AuNPs in 10% FBS or CCM protects the core materials from nonspecific attractions and prevents aggregation. Using PEGylated and zwitterion presenting DHLA ligands does not affect the appearance of the absorption properties of the NP dispersions, as nonspecific adsorption is essentially eliminated even in protein and salt rich media like 10% FBS, DMEM, and CCM.

Future ideas that we would like to explore include the use of multicoordinating polymers that either present negatively charged surface coatings or are modified with PEG blocks or zwitterion motifs. Using the same analytical techniques described here, one can probe whether or not electrostatically stabilized AuNPs with multicoordinating ligands can promote corona formation and compare findings to those acquired for zwitterion or PEGylated coatings made of monomeric ligands. Other ideas to explore include the use of more complex gold nanocolloids such as larger size nanorods and nanostars, surface-stabilized with these designed ligands. These may show behaviors that are different from those measured for simple spherical nanoparticles.

https://doi.org/10.1021/acsnano.3c08005
ACS Nano 2024, 18, 8649−8662

4. EXPERIMENTAL SECTION

4.1. Growth of Gold Nanoparticles (AuNPs). *4.1.1. Growth of Oleylamine-Capped AuNPs.* The 10 nm diameter oleylamine-coated AuNPs used in this study were synthesized by rapidly injecting $HAuCl_4$ precursors into a preheated oleylamine solution, as reported by Swihart and co-workers.[58] Briefly, 4 mL of oleylamine (OA) was refluxed at 150 °C under a nitrogen atmosphere using a 100 mL three-neck round-bottom flask. A mixture of 0.3 mmol (119 mg) of $HAuCl_4{\cdot}3H_2O$ dissolved in 2 mL of oleylamine was rapidly injected into the above flask. The reaction mixture was left to react at 150 °C for 1.5 h, yielding a brown pinkish color solution which indicates the formation of AuNPs. One round of centrifugation/purification was applied to remove unreacted precursors. The supernatant was collected, further diluted with hexane (10−15 mL), and then stored until further use. This growth route has yielded 10 nm diameter spherical AuNPs as verified by TEM measurements.[17,58,59] The 10 nm AuNPs prepared using this route were used for the gel electrophoresis measurements and for acquiring the light scattering data.

4.1.2. Growth of Citrate-Stabilized AuNPs. 4.1.2.1. Growth of 5 and 10 nm Diameter Spherical Nanoparticles. The 5 and 10 nm (diameter) citrate gold nanoparticles used in this study were prepared using a seeded-growth method using tannic acid and sodium citrate reducing agents, as reported by Puntes and co-workers.[61] The starting 3.5 nm Au seed solution was prepared as follows: 1 mL of tetrachloroauric acid ($HAuCl_4$, 25 mM) in DI water was injected into a solution containing a mixture of sodium citrate (150 mL, 2.2 mM), tannic acid (0.1 mL, 2.5 mM), and potassium carbonate (1 mL, 150 mM) heated at 70 °C. The reaction was left to progress for 5 min and then rapidly cooled down using an ice bath. To grow the nanoparticles, 55 mL of the seed solution (above) was mixed with an equal volume (55 mL) of 2.2 mM sodium citrate solution, then heated. When the solution reached 70 °C, two aliquots of $HAuCl_4$ (0.5 mL, 25 mM) were added at 10 min intervals. This step was repeated two times when growing 5 nm NPs and four times when growing 10 nm NPs. The final AuNP dispersion was concentrated by applying one round of centrifugation at 3500 rpm using a membrane centrifugation device with a MW cutoff = 50 kDa (Millipore). These AuNPs were used for gel electrophoresis and stability tests in biological media (e.g., 10% FBS).

4.1.2.2. Growth of 30 nm Diameter Spherical AuNPs. The 30 nm citrate-AuNPs used here were grown following the procedure reported by Puntes and co-workers.[60] Briefly, an initial solution of Au seeds was prepared by rapid injection of 1 mL of $HAuCl_4$ (25 mM in water) into a boiling aqueous solution of sodium citrate tribasic (150 mL, 2.2 m, using a round-bottom flask). The reaction was left to proceed for 10 min, until the AuNP dispersion color turned a red wine color, and then was stopped by cooling the flask content to room temperature. The reaction was heated up again to 90 °C, and then 1 mL of sodium citrate solution (60 mM) was injected followed by a second injection of 1 mL of $HAuCl_4$ solution (25 mM) after 2 min. The reaction was left to proceed while stirring for 30 min. The above steps (two injections and 30 min of stirring) were repeated 13 times, yielding 30 nm citrate-stabilized AuNPs. Growth of the NPs after each cycle was tracked/monitored using DLS measurements.

4.2. Ligand Synthesis. The polyethylene glycol-appended lipoic acid ligands used in this study, namely, LA-PEG_{750}-OCH_3, LA-$PEG_{600/1000}$-NH_2, and LA-$PEG_{600/1000}$-COOH, were prepared, characterized, and purified using the procedures described in previous reports.[102,103] Similarly, LA appended with zwitterion (N,N-dimethylpropanediamine-sulfobetaine) ligands was synthesized following the rationale described in references 104 and 105. Chemical reduction of the dithiolane group in the above compounds to DHLA was carried out using sodium borohydride, yielding PEG and zwitterion-appended DHLA, as reported in reference 102. These ligands were used for cap exchange of as-grown oleylamine- and citrate-capped AuNPs.

ASSOCIATED CONTENT

Supporting Information

The Supporting Information is available free of charge at https://pubs.acs.org/doi/10.1021/acsnano.3c08005.

Materials, instrumentation, methods, growth of the various surface-stabliized AuNPs, ligand exchange, gel electrophoresis (PDF)

AUTHOR INFORMATION

Corresponding Author

Hedi Mattoussi − *Department of Chemistry and Biochemistry, Florida State University, Tallahassee, Florida 32306, United States;* orcid.org/0000-0002-6511-9323; Email: mattoussi@chem.fsu.edu

Authors

Narjes Dridi − *Department of Chemistry and Biochemistry, Florida State University, Tallahassee, Florida 32306, United States;* orcid.org/0000-0001-9267-5475

Zhicheng Jin − *Department of Chemistry and Biochemistry, Florida State University, Tallahassee, Florida 32306, United States;* Present Address: Department of NanoEngineering, University of California, San Diego, La Jolla, CA 92093, United States; orcid.org/0000-0001-6072-7533

Woody Perng − *Department of Chemistry and Biochemistry, Florida State University, Tallahassee, Florida 32306, United States;* Present Address: Roche Inc., Indianapolis, IN, USA

Complete contact information is available at: https://pubs.acs.org/10.1021/acsnano.3c08005

Notes

The authors declare no competing financial interest.

ACKNOWLEDGMENTS

The authors thank FSU and the National Science Foundation (NSF-CHE, Grant #2005079), AFOSR (Grant No. FA9550-18-1-0144), the National Institutes of Health (RO1DK133464), and Kasei-Asahi Corporation for financial support. We also thank Goutam Palui and Wentao Wang for their suggestions and fruitful discussions.

REFERENCES

(1) Saha, K.; Agasti, S. S.; Kim, C.; Li, X. N.; Rotello, V. M. Gold Nanoparticles in Chemical and Biological Sensing. *Chem. Rev.* **2012**, *112*, 2739−2779.

(2) Zhou, W.; Gao, X.; Liu, D.; Chen, X. Gold Nanoparticles for In Vitro Diagnostics. *Chem. Rev.* **2015**, *115*, 10575−636.

(3) Wang, W.; van Niekerk, E. A.; Zhang, Y.; Du, L.; Ji, X.; Wang, S.; Baker, J. D.; Groeniger, K.; Raymo, F. M.; Mattoussi, H. Compact, "Clickable" Quantum Dots Photoligated with Multifunctional Zwitterionic Polymers for Immunofluorescence and In Vivo Imaging. *Bioconjugate Chem.* **2020**, *31*, 1497−1509.

(4) Fan, W.; Yung, B.; Huang, P.; Chen, X. Nanotechnology for Multimodal Synergistic Cancer Therapy. *Chem. Rev.* **2017**, *117*, 13566−13638.

(5) Wu, X.; Hao, C.; Kumar, J.; Kuang, H.; Kotov, N. A.; Liz-Marzan, L. M.; Xu, C. Environmentally responsive plasmonic nanoassemblies for biosensing. *Chem. Soc. Rev.* **2018**, *47*, 4677−4696.

(6) Yeasmin, S.; Ammanath, G.; Ali, Y.; Boehm, B. O.; Yildiz, U. H.; Palaniappan, A.; Liedberg, B. Colorimetric Urinalysis for On-Site Detection of Metabolic Biomarkers. *ACS Appl. Mater. Interfaces* **2020**, *12*, 31270−31281.

(7) Buss, C. G.; Bhatia, S. N. Nanoparticle delivery of immunostimulatory oligonucleotides enhances response to check-

point inhibitor therapeutics. *Proc. Natl. Acad. Sci. U.S.A.* **2020**, *117*, 13428−13436.
(8) Bodelon, G.; Montes-Garcia, V.; Lopez-Puente, V.; Hill, E. H.; Hamon, C.; Sanz-Ortiz, M. N.; Rodal-Cedeira, S.; Costas, C.; Celiksoy, S.; Perez-Juste, I.; Scarabelli, L.; La Porta, A.; Perez-Juste, J.; Pastoriza-Santos, I.; Liz-Marzan, L. M. Detection and imaging of quorum sensing in Pseudomonas aeruginosa biofilm communities by surface-enhanced resonance Raman scattering. *Nat. Mater.* **2016**, *15*, 1203−1211.
(9) Jain, P. K.; Huang, X. H.; El-Sayed, I. H.; El-Sayed, M. A. Noble Metals on the Nanoscale: Optical and Photothermal Properties and Some Applications in Imaging, Sensing, Biology, and Medicine. *Acc. Chem. Res.* **2008**, *41*, 1578−1586.
(10) Amendola, V.; Pilot, R.; Frasconi, M.; Marago, O. M.; Iati, M. A. Surface plasmon resonance in gold nanoparticles: a review. *J. Phys.: Condens. Matter* **2017**, *29*, 203002.
(11) Jin, Z.; Mantri, Y.; Retout, M.; Cheng, Y.; Zhou, J.; Jorns, A.; Fajtova, P.; Yim, W.; Moore, C.; Xu, M.; Creyer, M. N.; Borum, R. M.; Zhou, J.; Wu, Z.; He, T.; Penny, W. F.; O'Donoghue, A. J.; Jokerst, J. V. A Charge-Switchable Zwitterionic Peptide for Rapid Detection of SARS-CoV-2 Main Protease. *Angew. Chem., Int. Ed.* **2022**, *61*, No. e202112995.
(12) Jain, P. K.; Huang, X.; El-Sayed, I. H.; El-Sayed, M. A. Review of Some Interesting Surface Plasmon Resonance-enhanced Properties of Noble Metal Nanoparticles and Their Applications to Biosystems. *Plasmonics* **2007**, *2*, 107−118.
(13) Jin, Z.; Kapur, A.; Wang, W.; Diaz Hernandez, J.; Thakur, M.; Mattoussi, H. The dual-function of lipoic acid groups as surface anchors and sulfhydryl reactive sites on polymer-stabilized QDs and Au nanocolloids. *J. Chem. Phys.* **2019**, *151*, 164703.
(14) Jin, Z.; Yeung, J.; Zhou, J.; Cheng, Y.; Li, Y.; Mantri, Y.; He, T.; Yim, W.; Xu, M.; Wu, Z.; Fajtova, P.; Creyer, M. N.; Moore, C.; Fu, L.; Penny, W. F.; O'Donoghue, A. J.; Jokerst, J. V. Peptidic Sulfhydryl for Interfacing Nanocrystals and Subsequent Sensing of SARS-CoV-2 Protease. *Chem. Mater.* **2022**, *34*, 1259−1268.
(15) Wang, W.; Mattoussi, H. Engineering the Bio-Nano Interface Using a Multifunctional Coordinating Polymer Coating. *Acc. Chem. Res.* **2020**, *53*, 1124−1138.
(16) Heuer-Jungemann, A.; Feliu, N.; Bakaimi, I.; Hamaly, M.; Alkilany, A.; Chakraborty, I.; Masood, A.; Casula, M. F.; Kostopoulou, A.; Oh, E.; Susumu, K.; Stewart, M. H.; Medintz, I. L.; Stratakis, E.; Parak, W. J.; Kanaras, A. G. The Role of Ligands in the Chemical Synthesis and Applications of Inorganic Nanoparticles. *Chem. Rev.* **2019**, *119*, 4819−4880.
(17) Jin, Z.; Sugiyama, Y.; Zhang, C.; Palui, G.; Xin, Y.; Du, L.; Wang, S.; Dridi, N.; Mattoussi, H. Rapid Photoligation of Gold Nanocolloids with Lipoic Acid-Based Ligands. *Chem. Mater.* **2020**, *32*, 7469−7483.
(18) Bertoli, F.; Garry, D.; Monopoli, M. P.; Salvati, A.; Dawson, K. A. The Intracellular Destiny of the Protein Corona: A Study on its Cellular Internalization and Evolution. *ACS Nano* **2016**, *10*, 10471−10479.
(19) Ke, P. C.; Lin, S.; Parak, W. J.; Davis, T. P.; Caruso, F. A Decade of the Protein Corona. *ACS Nano* **2017**, *11*, 11773−11776.
(20) Fleming, A.; Cursi, L.; Behan, J. A.; Yan, Y.; Xie, Z.; Adumeau, L.; Dawson, K. A. Designing Functional Bionanoconstructs for Effective In Vivo Targeting. *Bioconjugate Chem.* **2022**, *33*, 429−443.
(21) Debayle, M.; Balloul, E.; Dembele, F.; Xu, X.; Hanafi, M.; Ribot, F.; Monzel, C.; Coppey, M.; Fragola, A.; Dahan, M.; Pons, T.; Lequeux, N. Zwitterionic polymer ligands: an ideal surface coating to totally suppress protein-nanoparticle corona formation? *Biomaterials* **2019**, *219*, 119357.
(22) Lynch, I.; Dawson, K. A. Protein-nanoparticle interactions. *Nano Today* **2008**, *3*, 40−47.
(23) Lundqvist, M.; Stigler, J.; Elia, G.; Lynch, I.; Cedervall, T.; Dawson, K. A. Nanoparticle size and surface properties determine the protein corona with possible implications for biological impacts. *Proc. Natl. Acad. Sci. U. S. A.* **2008**, *105*, 14265−14270.
(24) Perng, W.; Palui, G.; Wang, W.; Mattoussi, H. Elucidating the Role of Surface Coating in the Promotion or Prevention of Protein Corona around Quantum Dots. *Bioconjugate Chem.* **2019**, *30*, 2469−2480.
(25) Monopoli, M. P.; Walczyk, D.; Campbell, A.; Elia, G.; Lynch, I.; Baldelli Bombelli, F.; Dawson, K. A. Physical-Chemical Aspects of Protein Corona: Relevance to in Vitro and in Vivo Biological Impacts of Nanoparticles. *J. Am. Chem. Soc.* **2011**, *133*, 2525−2534.
(26) Walkey, C. D.; Olsen, J. B.; Guo, H.; Emili, A.; Chan, W. C. W. Nanoparticle Size and Surface Chemistry Determine Serum Protein Adsorption and Macrophage Uptake. *J. Am. Chem. Soc.* **2012**, *134*, 2139−2147.
(27) Monopoli, M. P.; Åberg, C.; Salvati, A.; Dawson, K. A. Biomolecular coronas provide the biological identity of nanosized materials. *Nat. Nanotechnol.* **2012**, *7*, 779−786.
(28) del Pino, P.; Pelaz, B.; Zhang, Q.; Maffre, P.; Nienhaus, G. U.; Parak, W. J. Protein corona formation around nanoparticles - from the past to the future. *Mater. Horiz.* **2014**, *1*, 301−313.
(29) Hamad-Schifferli, K. How can we exploit the protein corona? *Nanomedicine* **2013**, *8*, 1−3.
(30) Lynch, I.; Cedervall, T.; Lundqvist, M.; Cabaleiro-Lago, C.; Linse, S.; Dawson, K. A. The nanoparticle-protein complex as a biological entity; a complex fluids and surface science challenge for the 21st century. *Adv. Funct. Mater.* **2007**, *134*−*135*, 167−174.
(31) Caracciolo, G.; Farokhzad, O. C.; Mahmoudi, M. Biological Identity of Nanoparticles In Vivo: Clinical Implications of the Protein Corona. *Trends in Biotechnol.* **2017**, *35*, 257−264.
(32) Walczyk, D.; Bombelli, F. B.; Monopoli, M. P.; Lynch, I.; Dawson, K. A. What the Cell "Sees" in Bionanoscience. *J. Am. Chem. Soc.* **2010**, *132*, 5761−5768.
(33) Docter, D.; Westmeier, D.; Markiewicz, M.; Stolte, S.; Knauer, S. K.; Stauber, R. H. The nanoparticle biomolecule corona: lessons learned - challenge accepted? *Chem. Soc. Rev.* **2015**, *44*, 6094−6121.
(34) Salvati, A.; Pitek, A. S.; Monopoli, M. P.; Prapainop, K.; Bombelli, F. B.; Hristov, D. R.; Kelly, P. M.; Åberg, C.; Mahon, E.; Dawson, K. A. Transferrin-functionalized nanoparticles lose their targeting capabilities when a biomolecule corona adsorbs on the surface. *Nat. Nanotechnol.* **2013**, *8*, 137−143.
(35) Pozzi, D.; Colapicchioni, V.; Caracciolo, G.; Piovesana, S.; Capriotti, A. L.; Palchetti, S.; De Grossi, S.; Riccioli, A.; Amenitsch, H.; Laganà, A. Effect of polyethyleneglycol (PEG) chain length on the bio-nano-interactions between PEGylated lipid nanoparticles and biological fluids: from nanostructure to uptake in cancer cells. *Nanoscale* **2014**, *6*, 2782−2792.
(36) Chandran, P.; Riviere, J. E.; Monteiro-Riviere, N. A. Surface chemistry of gold nanoparticles determines the biocorona composition impacting cellular uptake, toxicity and gene expression profiles in human endothelial cells. *Nanotoxicology* **2017**, *11*, 507−519.
(37) Cheng, X.; Tian, X.; Wu, A.; Li, J.; Tian, J.; Chong, Y.; Chai, Z.; Zhao, Y.; Chen, C.; Ge, C. Protein Corona Influences Cellular Uptake of Gold Nanoparticles by Phagocytic and Nonphagocytic Cells in a Size-Dependent Manner. *ACS Appl. Mater. Interfaces* **2015**, *7*, 20568−75.
(38) Tenzer, S.; Docter, D.; Kuharev, J.; Musyanovych, A.; Fetz, V.; Hecht, R.; Schlenk, F.; Fischer, D.; Kiouptsi, K.; Reinhardt, C.; Landfester, K.; Schild, H.; Maskos, M.; Knauer, S. K.; Stauber, R. H. Rapid formation of plasma protein corona critically affects nanoparticle pathophysiology. *Nat. Nanotechnol.* **2013**, *8*, 772−781.
(39) Pelaz, B.; del Pino, P.; Maffre, P.; Hartmann, R.; Gallego, M.; Rivera-Fernández, S.; de la Fuente, J. M.; Nienhaus, G. U.; Parak, W. J. Surface Functionalization of Nanoparticles with Polyethylene Glycol: Effects on Protein Adsorption and Cellular Uptake. *ACS Nano* **2015**, *9*, 6996−7008.
(40) Mahmoudi, M.; Abdelmonem, A. M.; Behzadi, S.; Clement, J. H.; Dutz, S.; Ejtehadi, M. R.; Hartmann, R.; Kantner, K.; Linne, U.; Maffre, P.; Metzler, S.; Moghadam, M. K.; Pfeiffer, C.; Rezaei, M.; Ruiz-Lozano, P.; Serpooshan, V.; Shokrgozar, M. A.; Nienhaus, G. U.; Parak, W. J. Temperature: The "Ignored" Factor at the NanoBio Interface. *ACS Nano* **2013**, *7*, 6555−6562.

https://doi.org/10.1021/acsnano.3c08005
ACS Nano 2024, 18, 8649−8662

(41) Piella, J.; Bastus, N. G.; Puntes, V. Size-Dependent Protein-Nanoparticle Interactions in Citrate-Stabilized Gold Nanoparticles: The Emergence of the Protein Corona. *Bioconjugate Chem.* **2017**, *28*, 88−97.
(42) Rampado, R.; Crotti, S.; Caliceti, P.; Pucciarelli, S.; Agostini, M. Recent Advances in Understanding the Protein Corona of Nanoparticles and in the Formulation of "Stealthy" Nanomaterials. *Front. Bioeng. Biotechnol.* **2020**, *8*, 166.
(43) Lundqvist, M.; Augustsson, C.; Lilja, M.; Lundkvist, K.; Dahlback, B.; Linse, S.; Cedervall, T. The nanoparticle protein corona formed in human blood or human blood fractions. *PLoS One* **2017**, *12*, No. e0175871.
(44) Turner, J. G.; Murphy, C. J. How Do Proteins Associate with Nanoscale Metal-Organic Framework Surfaces? *Langmuir* **2021**, *37*, 9910−9919.
(45) Johnston, B. D.; Kreyling, W. G.; Pfeiffer, C.; Schäffler, M.; Sarioglu, H.; Ristig, S.; Hirn, S.; Haberl, N.; Thalhammer, S.; Hauck, S. M.; Semmler-Behnke, M.; Epple, M.; Hühn, J.; Del Pino, P.; Parak, W. J. Colloidal Stability and Surface Chemistry Are Key Factors for the Composition of the Protein Corona of Inorganic Gold Nanoparticles. *Adv. Funct. Mater.* **2017**, *27*, 1701956.
(46) Zhang, X.; Pandiakumar, A. K.; Hamers, R. J.; Murphy, C. J. Quantification of Lipid Corona Formation on Colloidal Nanoparticles from Lipid Vesicles. *Anal. Chem.* **2018**, *90*, 14387−14394.
(47) Grundler, J.; Shin, K.; Suh, H. W.; Zhong, M.; Saltzman, W. M. Surface Topography of Polyethylene Glycol Shell Nanoparticles Formed from Bottlebrush Block Copolymers Controls Interactions with Proteins and Cells. *ACS Nano* **2021**, *15*, 16118−16129.
(48) García, K. P.; Zarschler, K.; Barbaro, L.; Barreto, J. A.; O'Malley, W.; Spiccia, L.; Stephan, H.; Graham, B. Zwitterionic-Coated "Stealth" Nanoparticles for Biomedical Applications: Recent Advances in Countering Biomolecular Corona Formation and Uptake by the Mononuclear Phagocyte System. *Small* **2014**, *10*, 2516−2529.
(49) Safavi-Sohi, R.; Maghari, S.; Raoufi, M.; Jalali, S. A.; Hajipour, M. J.; Ghassempour, A.; Mahmoudi, M. Bypassing Protein Corona Issue on Active Targeting: Zwitterionic Coatings Dictate Specific Interactions of Targeting Moieties and Cell Receptors. *ACS Appl. Materials & Interfaces* **2016**, *8*, 22808−22818.
(50) García, I.; Sánchez-Iglesias, A.; Henriksen-Lacey, M.; Grzelczak, M.; Penadés, S.; Liz-Marzán, L. M. Glycans as Biofunctional Ligands for Gold Nanorods: Stability and Targeting in Protein-Rich Media. *J. Am. Chem. Soc.* **2015**, *137*, 3686−3692.
(51) Moyano, D. F.; Saha, K.; Prakash, G.; Yan, B.; Kong, H.; Yazdani, M.; Rotello, V. M. Fabrication of Corona-Free Nanoparticles with Tunable Hydrophobicity. *ACS Nano* **2014**, *8*, 6748−6755.
(52) Wei, H.; Insin, N.; Lee, J.; Han, H. S.; Cordero, J. M.; Liu, W. H.; Bawendi, M. G. Compact Zwitterion-Coated Iron Oxide Nanoparticles for Biological Applications. *Nano Lett.* **2012**, *12*, 22−25.
(53) Ren, J.; Andrikopoulos, N.; Velonia, K.; Tang, H.; Cai, R.; Ding, F.; Ke, P. C.; Chen, C. Chemical and Biophysical Signatures of the Protein Corona in Nanomedicine. *J. Am. Chem. Soc.* **2022**, *144*, 9184−9205.
(54) García-Álvarez, R.; Hadjidemetriou, M.; Sánchez-Iglesias, A.; Liz-Marzán, L. M.; Kostarelos, K. In vivo formation of protein corona on gold nanoparticles. The effect of their size and shape. *Nanoscale* **2018**, *10*, 1256−1264.
(55) Rodbard, D.; Chrambach, A. Unified theory for gel electrophoresis and gel filtration. *Proc. Natl. Acad. Sci. U S A* **1970**, *65*, 970−7.
(56) Park, S.; Brown, K. A.; Hamad-Schifferli, K. Changes in Oligonucleotide Conformation on Nanoparticle Surfaces by Modification with Mercaptohexanol. *Nano Lett.*. **2004**, *4*, 1925−1929.
(57) Pons, T.; Uyeda, H. T.; Medintz, I. L.; Mattoussi, H. Hydrodynamic dimensions, electrophoretic mobility, and stability of hydrophilic quantum dots. *J. Phys. Chem. B* **2006**, *110*, 20308−20316.
(58) Liu, S.; Chen, G.; Prasad, P. N.; Swihart, M. T. Synthesis of Monodisperse Au, Ag, and Au-Ag Alloy Nanoparticles with Tunable Size and Surface Plasmon Resonance Frequency. *Chem. Mater.* **2011**, *23*, 4098−4101.
(59) Nosratabad, N. A.; Jin, Z.; Du, L.; Thakur, M.; Mattoussi, H. N-Heterocyclic Carbene-Stabilized Gold Nanoparticles: Mono- Versus Multidentate Ligands. *Chem. Mater.* **2021**, *33*, 921−933.
(60) Bastus, N. G.; Comenge, J.; Puntes, V. Kinetically Controlled Seeded Growth Synthesis of Citrate-Stabilized Gold Nanoparticles of up to 200 nm: Size Focusing versus Ostwald Ripening. *Langmuir* **2011**, *27*, 11098−11105.
(61) Piella, J.; Bastús, N. G.; Puntes, V. Size-Controlled Synthesis of Sub-10-nanometer Citrate-Stabilized Gold Nanoparticles and Related Optical Properties. *Chem. Mater.* **2016**, *28*, 1066−1075.
(62) Turkevich, J.; Stevenson, P. C.; Hillier, J. A study of the nucleation and growth processes in the synthesis of colloidal gold. *Faraday Discuss.* **1951**, *11*, 55−75.
(63) Frens, G. Controlled Nucleation for Regulation of Particle-Size in Monodisperse Gold Suspensions. *Nature-Phys. Sci.* **1973**, *241*, 20−22.
(64) Alexis, F.; Pridgen, E.; Molnar, L. K.; Farokhzad, O. C. Factors affecting the clearance and biodistribution of polymeric nanoparticles. *Mol. Pharmaceutics* **2008**, *5*, 505−15.
(65) Owens, D. E., 3rd; Peppas, N. A. Opsonization, biodistribution, and pharmacokinetics of polymeric nanoparticles. *Int. J. Pharm.* **2006**, *307*, 93−102.
(66) Mei, B. C.; Oh, E.; Susumu, K.; Farrell, D.; Mountziaris, T. J.; Mattoussi, H. Effects of Ligand Coordination Number and Surface Curvature on the Stability of Gold Nanoparticles in Aqueous Solutions. *Langmuir* **2009**, *25*, 10604−10611.
(67) Mattoussi, H.; Mauro, J. M.; Goldman, E. R.; Anderson, G. P.; Sundar, V. C.; Mikulec, F. V.; Bawendi, M. G. Self-assembly of CdSe-ZnS quantum dot bioconjugates using an engineered recombinant protein. *J. Am. Chem. Soc.* **2000**, *122*, 12142−12150.
(68) Wang, W.; Ji, X.; Du, L.; Mattoussi, H. Enhanced Colloidal Stability of Various Gold Nanostructures Using a Multicoordinating Polymer Coating. *J. Phys. Chem. C* **2017**, *121*, 22901−22913.
(69) Turcu, I.; Zarafu, I.; Popa, M.; Chifiriuc, M. C.; Bleotu, C.; Culita, D.; Ghica, C.; Ionita, P. Lipoic Acid Gold Nanoparticles Functionalized with Organic Compounds as Bioactive Materials. *Nanomaterials (Basel)* **2017**, *7*, 43.
(70) Dzwonek, M.; Załubiniak, D.; Piątek, P.; Cichowicz, G.; Męczynska-Wielgosz, S.; Stępkowski, T.; Kruszewski, M.; Więckowska, A.; Bilewicz, R. Towards potent but less toxic nanopharmaceuticals - lipoic acid bioconjugates of ultrasmall gold nanoparticles with an anticancer drug and addressing unit. *RSC Adv.* **2018**, *8*, 14947−14957.
(71) Kapur, A.; Medina, S. H.; Wang, W.; Palui, G.; Schneider, J. P.; Mattoussi, H. Intracellular Delivery of Gold Nanocolloids Promoted by a Chemically Conjugated Anticancer Peptide. *ACS Omega* **2018**, *3*, 12754−12762.
(72) Dixit, V.; Van den Bossche, J.; Sherman, D. M.; Thompson, D. H.; Andres, R. P. Synthesis and grafting of thioctic acid-PEG-folate conjugates onto Au nanoparticles for selective targeting of folate receptor-positive tumor cells. *Bioconjugate Chem.* **2006**, *17*, 603−609.
(73) Kalmodia, S.; Vandhana, S.; Tejaswini Rama, B. R.; Jayashree, B.; Sreenivasan Seethalakshmi, T.; Umashankar, V.; Yang, W.; Barrow, C. J.; Krishnakumar, S.; Elchuri, S. V. Bio-conjugation of antioxidant peptide on surface-modified gold nanoparticles: a novel approach to enhance the radical scavenging property in cancer cell. *Cancer Nanotechnology* **2016**, *7*, 1.
(74) Tiwari, P. M.; Vig, K.; Dennis, V. A.; Singh, S. R. Functionalized Gold Nanoparticles and Their Biomedical Applications. *Nanomaterials (Basel)* **2011**, *1*, 31−63.
(75) Pons, T.; Medintz, I. L.; Wang, X.; English, D. S.; Mattoussi, H. Solution-phase single quantum dot fluorescence resonance energy transfer. *J. Am. Chem. Soc.* **2006**, *128*, 15324−15331.
(76) Daraee, H.; Eatemadi, A.; Abbasi, E.; Fekri Aval, S.; Kouhi, M.; Akbarzadeh, A. Application of gold nanoparticles in biomedical and drug delivery. *Artif. Cells Nanomed. Biotechnol.* **2016**, *44*, 410−422.

https://doi.org/10.1021/acsnano.3c08005
ACS Nano 2024, 18, 8649−8662

(77) Fan, M.; Han, Y.; Gao, S.; Yan, H.; Cao, L.; Li, Z.; Liang, X. J.; Zhang, J. Ultrasmall gold nanoparticles in cancer diagnosis and therapy. *Theranostics* **2020**, *10*, 4944−4957.
(78) Li, K.; Li, D.; Li, C. H.; Zhuang, P.; Dai, C.; Hu, X.; Wang, D.; Liu, Y.; Mei, X.; Rotello, V. M. Efficient in vivo wound healing using noble metal nanoclusters. *Nanoscale* **2021**, *13*, 6531−6537.
(79) Hill, A. V. The possible effects of the aggregation of the molecules of hemoglobin on its dissociation curves. *J. Physiol.* **1910**, *40*, iv−vii.
(80) Bisswanger, H. Multiple Equilibria, Principles, and Derivations. *Enzyme Kinetics* **2017**, 1−26.
(81) Ferruz, N.; De Fabritiis, G. Binding Kinetics in Drug Discovery. *Mol. Inform.* **2016**, *35*, 216−226.
(82) Jans, H.; Liu, X.; Austin, L.; Maes, G.; Huo, Q. Dynamic Light Scattering as a Powerful Tool for Gold Nanoparticle Bioconjugation and Biomolecular Binding Studies. *Anal. Chem.* **2009**, *81*, 9425−9432.
(83) Berne, B. J.; Pecora, R. *Dynamic Light Scattering: with Applications to Chemistry, Biology, and Physics*; Dover Publications: Mineola, NY, 2000; p vii, 376.
(84) Atkins, P.; De Paula, J.; Keeler, J. *Atkins' Physical Chemistry*, 11th ed.; Oxford University Press: New York, 2017.
(85) Holdgate, G. A. Thermodynamics of binding interactions in the rational drug design process. *Expert Opin. Drug. Discovery* **2007**, *2*, 1103−1114.
(86) Coxeter, H. S. M. Close-packing and froth. *Illinois J. Math.* **1958**, *2*, 746−758.
(87) Zhou, Z.-Y.; Zou, R.-P.; Pinson, D.; Yu, A.-B. Dynamic Simulation of the Packing of Ellipsoidal Particles. *Ind. Eng. Chem. Res.* **2011**, *50*, 9787−9798.
(88) Wright, A. K.; Thompson, M. R. Hydrodynamic structure of bovine serum albumin determined by transient electric birefringence. *Biophys. J.* **1975**, *15*, 137−141.
(89) Khan, S.; Gupta, A.; Verma, N. C.; Nandi, C. K. Kinetics of protein adsorption on gold nanoparticle with variable protein structure and nanoparticle size. *J. Chem. Phys.* **2015**, *143*, 164709.
(90) Chaudhary, A.; Gupta, A.; Khan, S.; Nandi, C. K. Morphological effect of gold nanoparticles on the adsorption of bovine serum albumin. *Phys. Chem. Chem. Phys.* **2014**, *16*, 20471−20482.
(91) Chakraborti, S.; Joshi, P.; Chakravarty, D.; Shanker, V.; Ansari, Z. A.; Singh, S. P.; Chakrabarti, P. Interaction of Polyethyleneimine-Functionalized ZnO Nanoparticles with Bovine Serum Albumin. *Langmuir* **2012**, *28*, 11142−11152.
(92) Welsch, N.; Lu, Y.; Dzubiella, J.; Ballauff, M. Adsorption of proteins to functional polymeric nanoparticles. *Polymer* **2013**, *54*, 2835−2849.
(93) Prozeller, D.; Morsbach, S.; Landfester, K. Isothermal titration calorimetry as a complementary method for investigating nanoparticle-protein interactions. *Nanoscale* **2019**, *11*, 19265−19273.
(94) Kabiri, M.; Unsworth, L. D. Application of Isothermal Titration Calorimetry for Characterizing Thermodynamic Parameters of Biomolecular Interactions: Peptide Self-Assembly and Protein Adsorption Case Studies. *Biomacromolecules* **2014**, *15*, 3463−3473.
(95) Silin, V. V.; Weetall, H.; Vanderah, D. J. SPR Studies of the Nonspecific Adsorption Kinetics of Human IgG and BSA on Gold Surfaces Modified by Self-Assembled Monolayers (SAMs). *J. Colloid Interface Sci.* **1997**, *185*, 94−103.
(96) Xiao, W.; Xiong, J.; Zhang, S.; Xiong, Y.; Zhang, H.; Gao, H. Influence of ligands property and particle size of gold nanoparticles on the protein adsorption and corresponding targeting ability. *Int. J. Pharm.* **2018**, *538*, 105−111.
(97) Partikel, K.; Korte, R.; Stein, N. C.; Mulac, D.; Herrmann, F. C.; Humpf, H. U.; Langer, K. Effect of nanoparticle size and PEGylation on the protein corona of PLGA nanoparticles. *Eur. J. Pharm. Biopharm.* **2019**, *141*, 70−80.
(98) Pearson, R. G. Hard and Soft Acids and Bases. *J. Am. Chem. Soc.* **1963**, *85*, 3533−3539.
(99) Uyeda, H. T.; Medintz, I. L.; Jaiswal, J. K.; Simon, S. M.; Mattoussi, H. Synthesis of compact multidentate ligands to prepare stable hydrophilic quantum dot fluorophores. *J. Am. Chem. Soc.* **2005**, *127*, 3870−3878.
(100) Schlenoff, J. B. Zwitteration: Coating Surfaces with Zwitterionic Functionality to Reduce Nonspecific Adsorption. *Langmuir* **2014**, *30*, 9625−9636.
(101) Boström, M.; Deniz, V.; Franks, G. V.; Ninham, B. W. Extended DLVO theory: Electrostatic and non-electrostatic forces in oxide suspensions. *Adv. Colloid Interface Sci.* **2006**, *123*−*126*, 5−15.
(102) Susumu, K.; Mei, B. C.; Mattoussi, H. Multifunctional ligands based on dihydrolipoic acid and polyethylene glycol to promote biocompatibility of quantum dots. *Nat. Protocols* **2009**, *4*, 424−436.
(103) Mei, B. C.; Susumu, K.; Medintz, I. L.; Mattoussi, H. Polyethylene glycol-based bidentate ligands to enhance quantum dot and gold nanoparticle stability in biological media. *Nat. Protocols* **2009**, *4*, 412−423.
(104) Zhan, N.; Palui, G.; Grise, H.; Tang, H.; Alabugin, I.; Mattoussi, H. Combining Ligand Design with Photoligation to Provide Compact, Colloidally Stable, and Easy to Conjugate Quantum Dots. *ACS Appl. Mater. & Interfaces* **2013**, *5*, 2861−2869.
(105) Zhan, N.; Palui, G.; Mattoussi, H. Preparation of compact biocompatible quantum dots using multicoordinating molecular-scale ligands based on a zwitterionic hydrophilic motif and lipoic acid anchors. *Nat. Protocols* **2015**, *10*, 859−874.

https://doi.org/10.1021/acsnano.3c08005
ACS Nano 2024, 18, 8649−8662